ACSNANO

www.acsnano.org

ARTICLE

Biomimetic Surface-Enhanced Raman Scattering Nanoparticles with Improved Dispersibility, Signal Brightness, and Tumor Targeting Functions

Indrajit Srivastava, Ruiyang Xue, Jamie Jones, Hyunjoon Rhee, Kristen Flatt, Viktor Gruev,* and Shuming Nie*

Cite This: *ACS Nano* 2022, 16, 8051−8063

Read Online

ACCESS | Metrics & More | Article Recommendations | Supporting Information

ABSTRACT: The development of biocompatible and nontoxic surface-enhanced Raman scattering (SERS) nanoparticles is of considerable current interest because of their attractive biomedical applications such as ultrasensitive in vitro diagnostics, in vivo tumor imaging, and spectroscopy-guided cancer surgery. However, current SERS nanoparticles are prepared and stored in aqueous solution, have limited stability and dispersibility, and are not suitable for lyophilization and storage by freeze-drying or other means. Here, we report a simple but robust method to coat colloidal SERS nanoparticles by naturally derived biomimetic red blood cell membranes (RBCM), leading to a dramatic improvement in stability and dispersibility under freeze−thawing, lyophilization, heating, and physiological conditions. The results demonstrate that the lyophilized SERS nanoparticles in the solid form can be readily dissolved and dispersed in physiological buffer solutions. A surprising finding is that the RBCM-coated SERS particles are considerably brighter (by as much as 5-fold) than PEGylated SERS particles under similar experimental conditions. This additional enhancement is believed to arise from the hydrophobic nature of RBCM's hydrocarbon chains, which is known to reduce electronic dampening and boost electromagnetic field enhancement. A further advantage in using biomimetic membrane coatings is that the bilayer membrane structure allows nonvalent insertion of molecular ligands for tumor targeting. In particular, we show that cyclic-RGD, a tumor-targeting peptide, can be efficiently inserted into the membrane coatings of SERS nanoparticles for targeting the $\alpha v\beta 3$ integrin receptors expressed on cancer cells. Thus, biomimetic RBCMs provide major advantages over traditional polyethylene glycols for preparing SERS nanoparticles with improved dispersibility, higher signal intensity, and more efficient biofunctionalization.

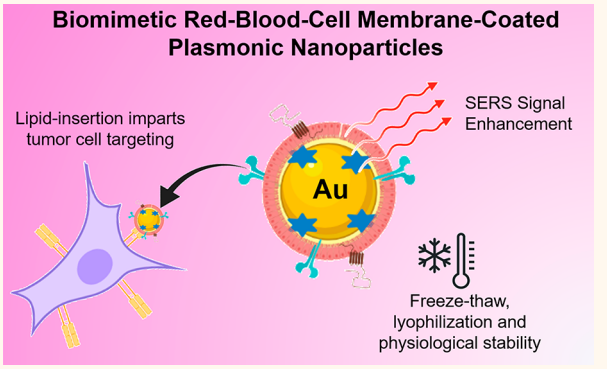

KEYWORDS: *red blood cell membrane, surface coatings, gold nanoparticles, dispersion stability, surface-enhanced Raman scattering, plasmonics, tumor targeting*

Gold nanoparticles (AuNPs) functionalized with Raman-active dye molecules have been extensively used as surface-enhanced Raman scattering (SERS) nanotags owing to their intriguing attributes of size and shape tunability, high photostability, low cytotoxicity, high biocompatibility, and narrow spectral bandwidth.[1−4] Recent advances have developed SERS nanoparticles (NPs) or nanotags for a multitude of biomedical applications including in vivo imaging, in vitro diagnostics, and image-guided cancer surgery.[5−11] A major component in these SERS nanotags is an external coating layer that serves several important purposes.[12] First, this coating layer prevents loss or leaching of the Raman reporter molecules into the surrounding media, hence avoiding toxicity issues and cross-contamination with vibrational signatures of other nanotags. Second, this layer minimizes

Received: January 30, 2022
Accepted: April 20, 2022
Published: April 26, 2022

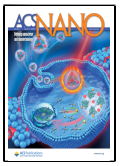

https://doi.org/10.1021/acsnano.2c01062
ACS Nano 2022, 16, 8051−8063

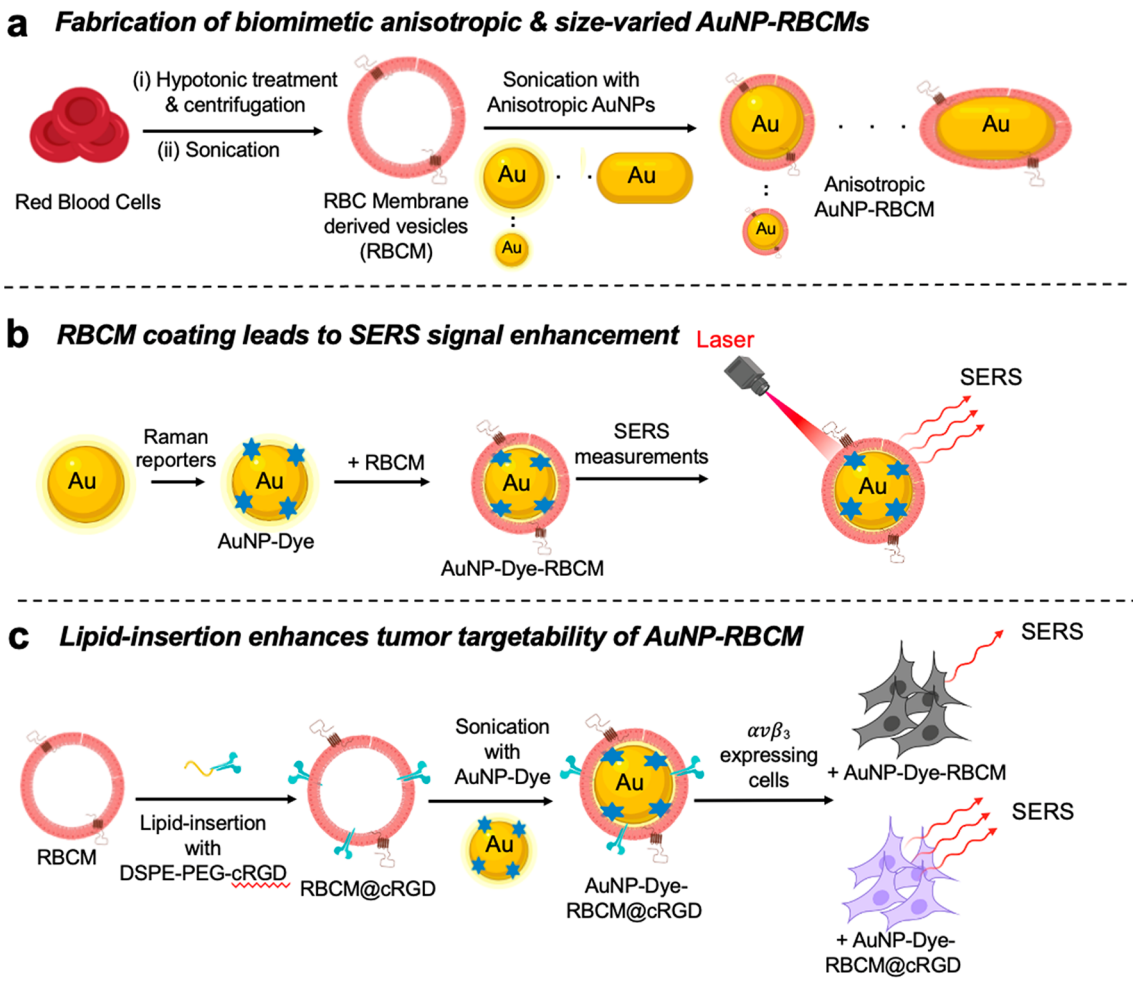

Figure 1. (a) Schematic diagram showing preparation of RBCM vesicles and successful coating on anisotropic AuNPs, leading to RBCM-coated AuNP-RBCM with enhanced dispersibility and biofunctionalization properties. (b) RBCM coating on dye-tagged AuNP leads to SERS signal enhancement and retains long-term signal stability in different storage conditions. (c) Lipid-insertion allows modifying the RBCM with tumor-targeting cRGD peptides, imparting the AuNP-RBCM constructs with cancer cell targetability and use as in vitro SERS nanotags.

the influence of other molecules present in the medium and prevents undesired intensity variations. Third, it also minimizes plasmonic coupling interactions between NPs which could lead to the uncontrolled generation of plasmonic hot spots. Fourth, this coating increases the colloidal stability of NPs and provides an outer layer for further chemical modification. The external coatings are often comprised of silica,[1−5] polymers,[6−10] or liposomes.[11−13] A silica coating has the advantage of biodegradability, but for long-term studies, it has been known to cause degradation and agglomeration problems. Polymers such as polyethylene glycol (PEG) have been extensively used for coating, but the ability of PEG coatings to prevent aggregation is limited in high ionic strength buffer solutions. Amphiphilic polymers have been recently utilized as a coating material for SERS nanotags based on hydrophobic interactions between the polymer and Raman reporter dye,[22,26] but these constructs have limited dispersion stability (irreversible aggregation upon freeze-drying), limiting their clinical translatability.[14−19] Recently, liposomes composed of zwitterionic phosphatidyl-choline lipid-coated SERS nanotags have been developed by several research groups.[11,20] These lipids mimic the natural cell membranes and possess advantageous functions of improved dispersibility, biocompatibility, and the potential of tumor cell targeting via antibody conjugation or lipid-functionalized antibody fragments. However, such artificial membranes are unable to recapitulate the structure or protein composition of natural cell membranes, including their intrinsic properties of homologous tumor targeting, enhanced blood circulation, etc.[21,22] Hence, coating NPs with naturally derived cell membranes is an interesting biomimetic engineering top-down approach[33−38] imparting NPs with properties of specific cell types. This approach overcomes the limitations of biomaterials designed specifically to mimic cell membranes via the bottom-up strategies. Biomimetic cell membrane-coated nanomaterials have been developed for drug delivery to treat cancer, microbial infections, etc.[23−26] However, to the best of our knowledge, biomimetic membranes have not been used to coat SERS nanotags, and it is not known how such cell membrane coatings might influence the SERS signal brightness and dispersion stability properties and how they could be modified to impart tumor targeting functions (Figure 1a−c).

Here, we demonstrate that biomimetic red blood cell membranes (RBCMs) can provide enhanced dispersion stability to AuNPs with varied shapes (sphere, rod, cube) and sizes (D_h ~15−80 nm). Specifically, we show that the

https://doi.org/10.1021/acsnano.2c01062
ACS Nano 2022, 16, 8051−8063

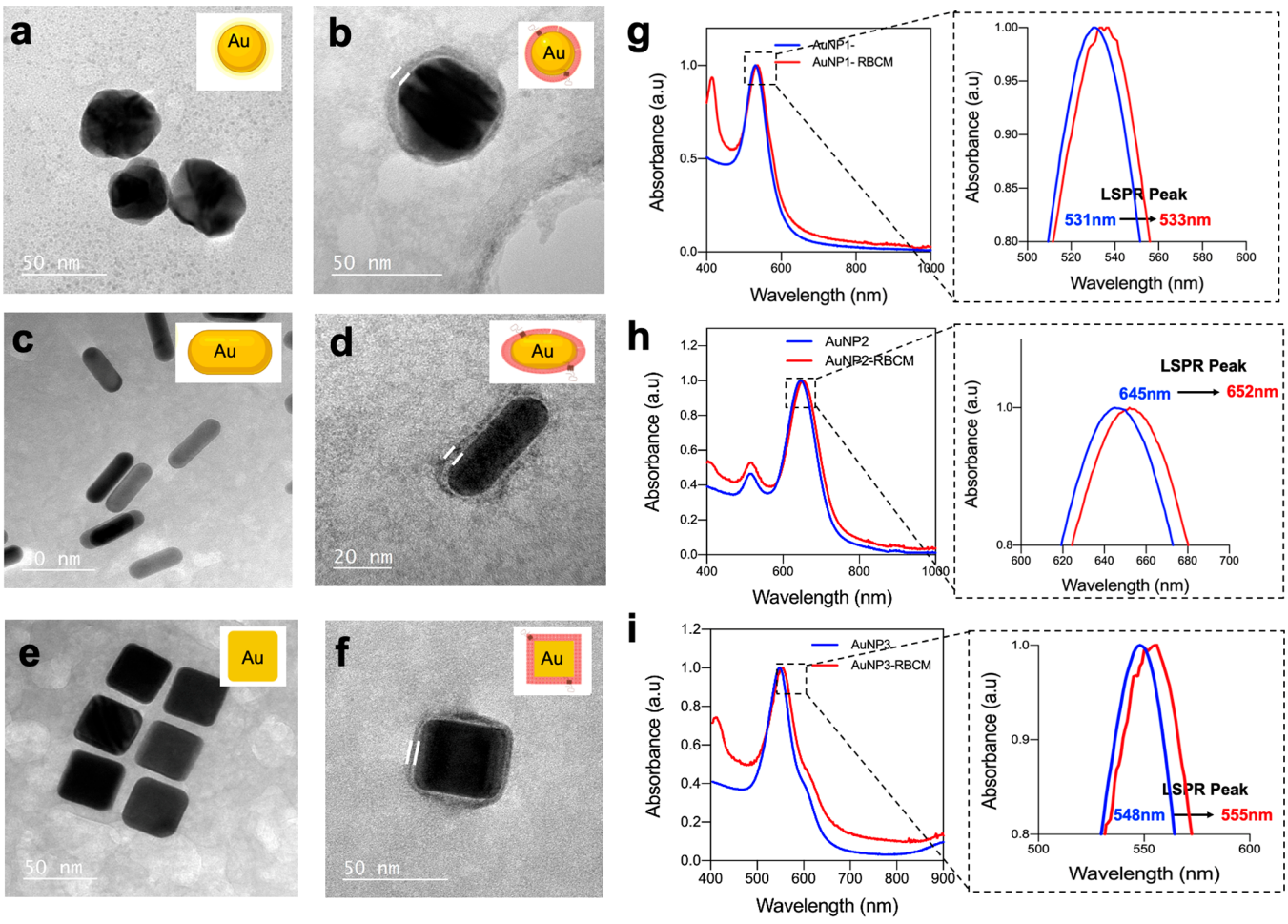

j

Samples	Hydrodynamic Diameter (nm)		Zeta Potential (mV)	
	-RBCM	+RBCM	-RBCM	+RBCM
AuNP1	44 ± 5	64 ± 4	-37 ± 6	-28 ± 3
AuNP2	54 ± 4	66 ± 4	-38 ± 6	-27 ± 4
AuNP3	53 ± 5	68 ± 4	-40 ± 6	-30± 2

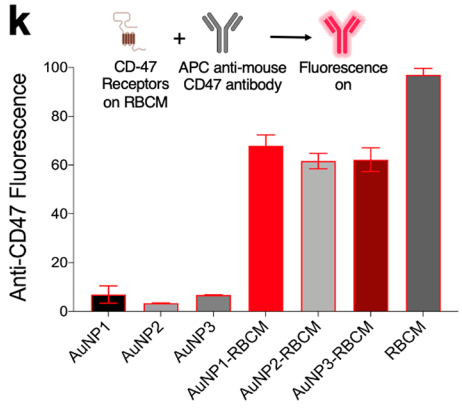

Figure 2. Physicochemical characterization of anisotropic RBCM-coated AuNPs. Negative-stained transmission electron micrographs of (a) AuNP1-Cit, (b) AuNP1-RBCM, (c) AuNP2-Cit, (d) AuNP2-RBCM, (e) AuNP3-Cit, and (f) AuNP3-RBCM, with the membrane coating in (b, d, f) highlighted with white lines. (g–i) UV–vis absorbance spectra of AuNP's and AuNP-RBCM's, with the inset boxes zoomed. The inset shows the intrinsic plasmonic absorbance peak shift for different anisotropic AuNPs upon RBCM coating. (j) Hydrodynamic diameter and ζ potential measurements for AuNPs before and after RBCM coating. (k) Anisotropic AuNPs uncoated and coated with RBCM were stained with a fluorescent anti-CD47 antibody. Data shown as mean ± standard deviation, *n* = 3.

RBCM coating strategy imparts AuNPs stability against lyophilization, freezing, heating, and under different physiological conditions. In addition, a noncovalent lipid-insertion strategy[27] could be adopted to functionalize these AuNP-RBCM with tumor targeting ligands. AuNP-RBCM do not lose their activity or stability upon further freeze–thaw cycles, establishing functionalization on RBCM with other proteins or molecules of interest. As such, the RBCM coating strategy on AuNPs imparts these constructs with enhanced dispersion stability with fast and efficient functionalization, enabling their long-term storage for biomedical and clinical applications which cannot be achieved by the current unstable surfactant stabilized or PEGylated AuNPs. In addition, the SERS signal intensities of RBCM-coated particles are considerably higher (by about 5) in comparison with that PEGylated AuNPs. This additional enhancement is most likely to arise from a hydrophobic environment effect (RBCM consists of a large number of lipid hydrocarbon chains) which reduces electronic

https://doi.org/10.1021/acsnano.2c01062
ACS Nano 2022, 16, 8051–8063

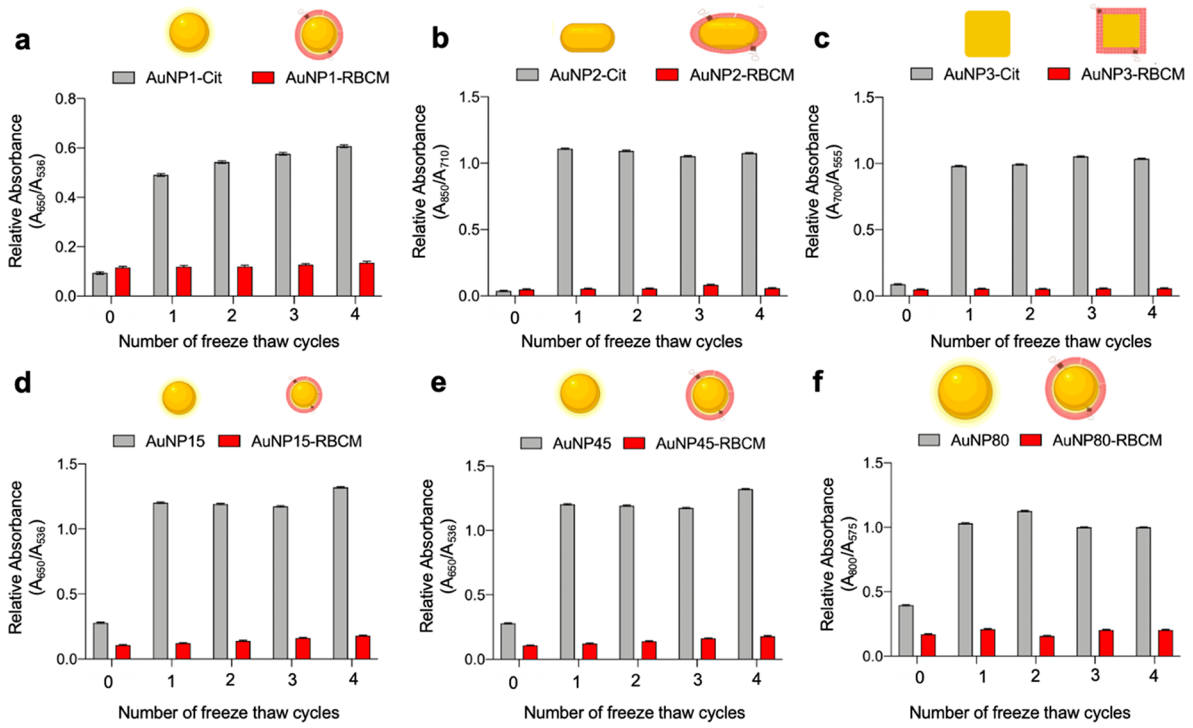

Figure 3. Comparison of the relative absorbances to evaluate the aggregation tendency during the freeze−thaw cycles for (a) AuNP1-Cit and AuNP1-RBCM, (b) AuNP2-Cit and AuNP2-RBCM, (c) AuNP3-Cit and AuNP3-RBCM, (d) AuNP15 and AuNP15-RBCM, (e) AuNP45 and AuNP45-RBCM, and (f) AuNP80 and AuNP80-RBCM.

dampening and boosts electromagnetic field enhancement. The improved SERS signals are well-protected by RBCM during freeze−thaw cycles and on long-term storage for 2 weeks. In a proof-of-concept study, we utilized a lipid-insertion strategy to conjugate tumor-targeting cyclic cRGD peptides onto these biomimetic SERS NPs so that they exhibited improved intracellular uptake in $\alpha v\beta 3$ integrin receptors expressing cells (MDA-MB231) with minimal cytotoxicity. These RBCM encapsulated SERS tags could be used for future in vitro and in vivo SERS detections with better sensitivity, signal stability, and long-term storage.

RESULTS AND DISCUSSION

Functionalization of AuNPs with Biomimetic RBCM. As illustrated in Figure 1a, the process of functionalizing AuNPs with mouse-derived RBC membranes was conducted by generating membrane vesicles from RBCs and subsequently fusing the RBC membranes onto the surface of AuNPs via bath sonication. First, RBC ghosts were derived from purified mouse RBCs via hypotonic treatment and centrifugation steps. Next, RBC membrane vesicles, RBCM (∼190 nm), were prepared using bath sonication. Subsequently, citrate-stabilized AuNPs (0.032 mg/mL) having different shapes (AuNP1: 45 nm Au sphere, AuNP2: rod, AuNP3: cube) and sizes (AuNP15: D_h 15 nm, AuNP45: D_h 45 nm, AuNP80: D_h 80 nm) were mixed with the RBC vesicles and bath sonicated resulting in the functionalization of AuNPs with RBC vesicles, referred as AuNP-RBCM. Throughout this work, AuNP or AuNP1 will refer to 45 nm AuNPs.

Characterization of AuNP-RBCM. To confirm the uniform coating onto AuNPs, transmission electron microscopy (TEM) was utilized for both bare-AuNPs and AuNP-RBCM (Figure 2a−f). Successful RBCM coating on anisotropic AuNPs was further monitored by changes in the hydrodynamic size and surface ζ potential of AuNPs before and after the functionalization process (Figure 2j). Following the membrane fusion process, the diameters of all AuNPs (size and shape varied) increased by ∼8−10 nm, indicating a uniform RBC membrane coating which agrees with previous reports.[28,29] UV−vis-NIR spectra were subsequently collected to investigate the intrinsic plasmon peak changes on anisotropic AuNPs before and after the RBCM coating process (Figure 2g-i). The intrinsic plasmon peak for AuNP-RBCM gradually red-shifted compared to AuNP: ∼2 nm for AuNP1 (531−533 ± 1 nm) and ∼7 nm for AuNP2 (645−652 ± 3 nm) and AuNP3 (548−555 ± 10 nm), respectively, which could be attributed to the diameter increase by the wrapping of RBCM. The surface ζ potential of AuNPs was also found to increase upon RBC membrane vesicle coating, possibly due to the less negative surface charge of RBC membranes when compared to citrate stabilized AuNPs, indicating that there was likely a charge screening.

We further performed an indirect study to confirm the successful RBCM coating on AuNPs by confirming the presence of CD47 proteins on the surface of the particles. CD47 protein is a "marker of self" receptor on the surface of RBCs which bind to the signal regulatory protein alpha receptors on macrophages and inhibit phagocytosis of RBCs. Consequently, the presence of CD47 on RBCM coated AuNPs would indicate successful functionalization without the loss in activity of the RBCMs.[30] Here, different samples including RBCM, AuNPs, and AuNP-RBCMs were mixed with fluorescent antibody for CD47, and we observed the highest fluorescent signal intensity for RBCM, followed by AuNP-RBCMs. The AuNPs had barely any signal intensity due to the lack of CD47 receptors on their surface (Figure 2k). Together,

https://doi.org/10.1021/acsnano.2c01062
ACS Nano 2022, 16, 8051−8063

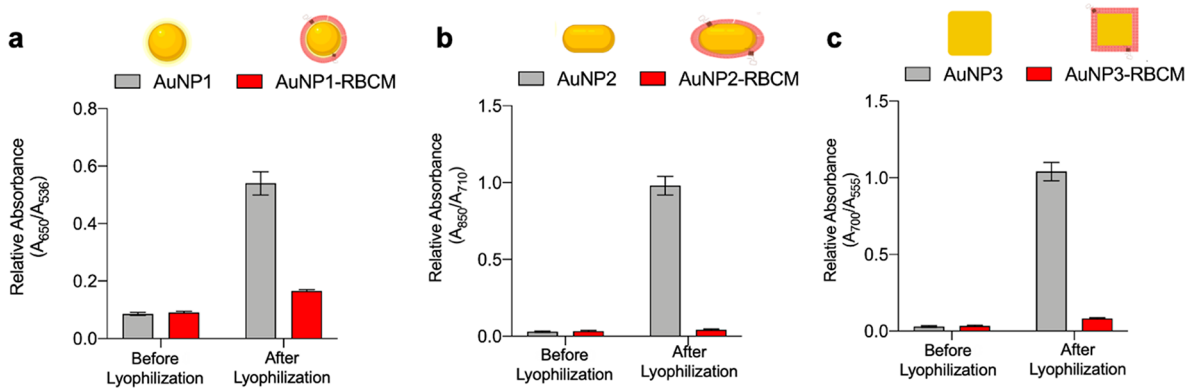

Figure 4. Comparison of the relative absorbances to evaluate the aggregation tendency during the lyophilization cycles for (a) AuNP1-Cit and AuNP-RBCM, (b) AuNP2-Cit and AuNP2-RBCM, and (c) AuNP3-Cit and AuNP3-RBCM.

these results indicate that both size- and shape-tuned AuNPs were successfully coated with RBC-derived membranes.

Dispersion Stability of AuNP-RBCM against Freezing, Lyophilization, Heating, and under Physiological Conditions. We proceeded to investigate the enhanced dispersion stability aspects imparted by the biomimetic AuNP-RBCM and compared it with citrate-stabilized AuNPs (AuNP-Cit) and linear PEG functionalized AuNPs (AuNP-PEG), which is used for biological applications.[17,31−34] We first investigated the freeze−thaw behavior of AuNP-RBCM by freezing them at −80 °C for 30 min, followed by thawing them at room temperature, repeating these freeze−thaw cycles 4 times (Figure 3). For AuNP-RBCM, the red color of the solution persisted, and the UV−vis showed identical spectra to that before freezing, demonstrating that the RBCM functionalization step provided enhanced dispersibility through the frozen state. AuNP-PEG demonstrated a similar behavior when subjected to freeze−thaw cycles. However, AuNP-Cit changed their color from red to colorless when subjected to freeze−thaw cycles with their UV−vis spectra showing that their plasmon absorption peak shifts to higher wavelengths and becomes broader. Hence, we calculated corresponding relative absorbance values to correlate with the stability of different AuNP samples upon the treatment. This trend was consistent across AuNPs having different shapes and sizes as evident by the relative absorbance calculations (Figure 3 and Figure S2). Hydrodynamic diameter measurements further showed an increase in size upon freeze−thaw cycles for AuNP-Cit, suggesting aggregation (Figure S4). However, AuNP-RBCM and AuNP-PEG did not show any noticeable change in hydrodynamic diameter and TEM upon freeze−thaw cycles (Figures S4 and S5).

Based on these results, we next attempted to evaluate the effects of lyophilization (Figure 4a−c and Figure S3). Here, the samples were frozen in liquid nitrogen followed by sublimation of the solvent under reduced pressure. AuNP1-RBCM maintained their red color, indicating they did not aggregate in the solid-state, suggesting that the RBCM coating prevented AuNP aggregation. Upon addition of DI water, AuNP1-RBCM was successfully redispersed giving a good restoration of the original UV−vis absorption signal. However, AuNP1-PEG and AuNP1-Cit upon redispersion in DI water gave a lighter red color and gray color, respectively, with a considerable shift in the surface plasmon resonance band of the AuNPs, indicating aggregation after lyophilization. Negative-stained TEM images were further performed that showed aggregation for AuNP1-Cit and AuNP1-PEG and no aggregation for AuNP1-RBCM (Figure S6). These experiments further consolidate the premise that RBCM coating on AuNPs endows them with superior dispersion stability against lyophilization and freeze−thaw treatments. We further demonstrated that changing the hydrodynamic diameter of AuNP1-RBCM to 15 and 80 nm did not affect the enhanced dispersion stability feature imparted by the RBCM membranes (Figures S7−S10).

Having dispersion stability against physiological conditions and high temperatures would be ideal for future applications in photothermal therapy when using these AuNP-RBCM constructs. Physiological conditions have salts including NaCl that cause unwanted aggregation owing to the enhanced ionic strength forming a salt between the citrate on AuNP surface, which neutralizes the charges.[35] After demonstrating the enhanced dispersibility of our RBCM coating on AuNPs, we next examined under different physiological conditions. The dispersibility of AuNP1-Cit, AuNP1-RBCM, and AuNP1-PEG was tested at physiological conditions of pH = 7.4 and ∼137 mM of NaCl. A phosphate buffer saline (PBS 10×) solution (0.1 mL) was added to the AuNP1/AuNP1-RBCM/AuNP1-PEG dispersions (1 mL) to make the desired physiological condition. The color of AuNP1-Cit instantaneously changed from dark red to colorless immediately after the addition of the concentrated PBS solution. On the other hand, no significant color change or aggregation (via UV−vis absorption) was observed for AuNP1-PEG and AuNP1-RBCM after 4 h of incubation (Figures S11 and S12).

Next, to determine their thermal stability, AuNP1-Cit, AuNP1-RBCM, and AuNP1-PEG were heated at 85 °C for 4 h (Figure S13). AuNP1-Cit eventually turned into an almost colorless liquid solution with aggregation, as depicted by their UV−vis absorption spectra. Both AuNP1-RBCM and AuNP1-PEG showed high stability by retaining their red color and no aggregation, as observed by their UV−vis absorption spectra. It was interesting to note during the heating, the protein peak due to RBCM slowly started to disintegrate, but it was still sufficient to maintain the AuNPs dispersibility.

Finally, we tested the stability of different AuNPs (AuNP1-Cit, AuNP1-RBCM, and AuNP1-PEG) in a biological fluid, that is, human serum. This will be an important prerequisite for AuNP1-RBCM that could allow different in vitro and in vivo biosensing and biomedical applications. Using dynamic light scattering (DLS) to measure their hydrodynamic diameter, we did not observe any aggregates for AuNP-RBCM (Figure S14). However, for AuNP-Cit and AuNP-PEG,

https://doi.org/10.1021/acsnano.2c01062
ACS Nano 2022, 16, 8051−8063

the hydrodynamic diameter gradually increased due to the formation of large aggregates, highlighting the importance of improved dispersibility provided by RBCM (Figure S14).

Design of Biomimetic SERS Nanoparticles with Signal Enhancement, Long-Term Signal, and Dispersion Stability. The biomimetic RBCM was coated on dye attached AuNPs to function as the protective coating of SERS NPs. The resulting SERS NPs were referred to as AuNP-dye-RBCM. Dye attached AuNPs without coating (AuNP-dye) and dye-attached AuNPs coated with 2k Da SH-PEG (AuNP-dye-PEG) were employed as controls. Raman spectra of different AuNPs were measured in aqueous NP solutions with the same particle concentration and laser parameter (integration time and laser power). It was first observed that, after RBCM coating, the SERS intensity increases to 5 times the original intensity of AuNP-dye (Figure 5a,b). Hotspot-induced SERS intensity change was excluded by good monodispersity of AuNP-dye-RBCM that is indicated in the absorbance spectrum and hydrodynamic size distribution (Figure S15). The compact wrapping of RBCM around AuNPs was proved to be important for the SERS enhancement by three supplementary trials (Figure S16). In the first trial, the AuNP-dye solution was simply mixed with RBCM fragments without bath sonication treatment. Only a ~3 times enhancement was observed after the mixing, which is probably due to membrane fragments attaching to AuNPs and forming an incomplete RBCM shell. The mixture was then treated with a 10 min bath sonication, and the SERS signal increases to 5 times the original intensity as a result of a complete and compact membrane packing (Figure S16a). In the second trial, the RBCM was coated on the surface of AuNP-dye-PEG (Figure S16b), and in the third trial, AuNPs were mixed with dye solution after RBCM coating (Figure S16c). None of these experiments resulted in a SERS intensity enhancement as high as directly attaching RBCM on dye absorbed AuNPs, indicating that a tight and direct encapsulation of RBCM on AuNPs is essential for the observed SERS enhancement. The enhancement effect is then believed to be related to the electromagnetic enhancement mechanism, where the dielectric medium around plasmonic NPs changing from polar water (dielectric constant of 80.4) to the nonpolar lipid bilayer (averaged dielectric constant of 2 to 3) leads to an amplified reduction of electron dampening and boosts the electromagnetic field enhancement (detailed mechanism discussed in Supporting Information).[36]

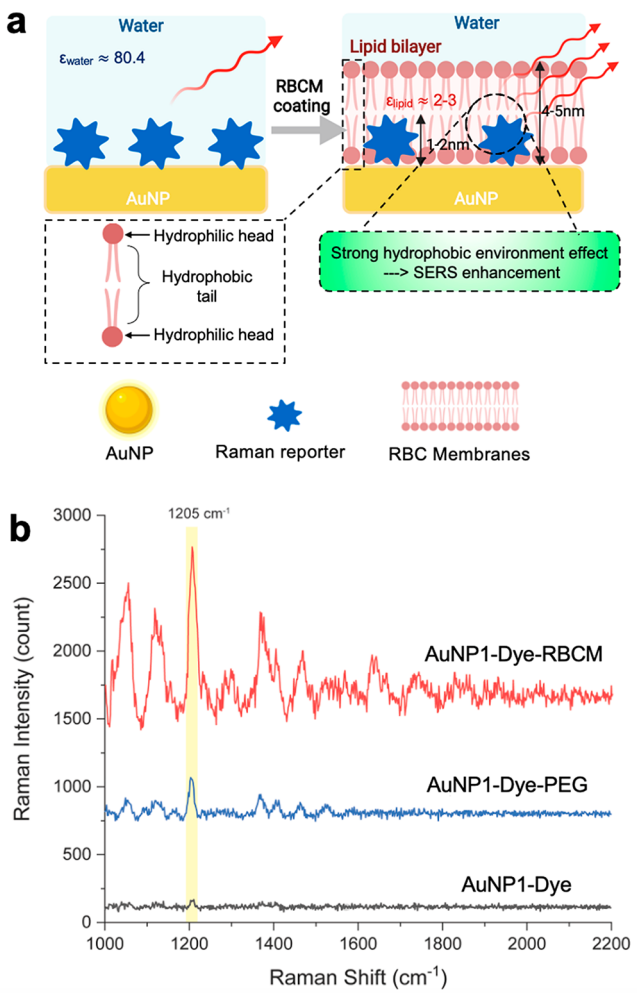

Figure 5. (a) Schematics depicting the hydrophobic structure of RBCM and surface Raman enhancement. The dielectric constant of the surrounding medium changes from 80.4 (water) to 2−3 (lipid bilayer), which leads to an amplified local electromagnetic field. (b) Raman spectra of AuNP1-dye, AuNP1-dye-PEG, and AuNP1-dye-RBCM, respectively, showing enhanced SERS intensity after RBCM coating. Spectra were acquired at a laser power of 200 mW and integration time of 500 ms.

Besides, the enhanced SERS signal was observed to be quite stable over time, as the intensity of AuNP-dye-RBCM stays ~90% after up to 2 month storage at 4 °C. Unfortunately, AuNP-dye-Cit irreversibly aggregated over this period. AuNP-Cit is generally stable for long-term storage due to its negative surface charge. However, after the attachment of the positively charged dye, the net surface charge of AuNP-Cit drops below −20 mV (Figure S17), and hence it is eventually aggregate during long-term storage. The SERS stability of AuNP-dye-RBCM was also tested during freeze−thaw cycles. RBCM exhibited excellent protection of SERS NPs against freezing, demonstrating not only well-preserved NPs dispersity but also a stable and intact SERS signal (Figure 6a−g). In contrast, obvious aggregation was observed in AuNP-dye-Cit upon freezing, leading to an uncontrolled SERS enhancement.[18,34] A plausible explanation could be that when SERS AuNPs begin to aggregate, SERS hotspots are generated between adjunct AuNPs, resulting in a strong electric field in the area that enhances the SERS intensity.[37] However, this increased SERS signal owing to chemical or physical property change of the solution system is undesirable because the hotspot generation does not happen in a controlled manner, leading to unrepeatable SERS enhancement.[38,39] Hence, upon subjection to freeze−thaw treatments, AuNP-Dye-Cit aggregate leads to its uncontrolled SERS enhancement.

Though AuNP-dye-PEG did not aggregate, it showed a continuous SERS intensity decrease with ongoing freeze−thaw cycles (Figure S18). We further demonstrated that upon lyophilization, AuNP-dye-RBCM retained its SERS spectra and corresponding intensities without any noticeable signs of aggregation. As expected, the AuNP dye aggregated upon lyophilization, as shown by its SERS spectra (Figure S19). The cryoprotection of dye reporter molecules and SERS brightness from RBCM are hypothesized to be related to the strong hydrophobic−hydrophobic interaction between aromatic dye molecules and the alkyl tails of the lipids. However, the exact mechanism remains unclear and requires further investigations.

https://doi.org/10.1021/acsnano.2c01062
ACS Nano 2022, 16, 8051−8063

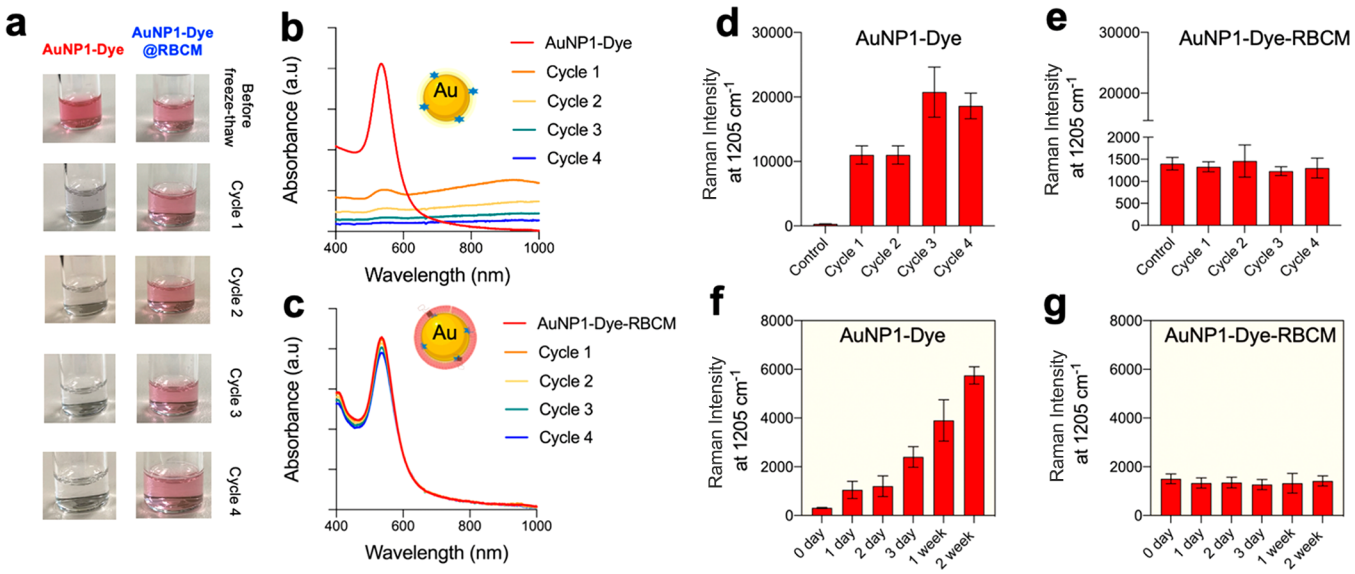

Figure 6. (a–g) Dispersion stability data before and after four successive freeze–thaw cycles. (a) Photographs. (b, c) UV–vis absorption spectra. (d, e) Plots of SERS signal intensities at 1205 cm^{-1} as a function of freeze–thaw cycle, showing superior dispersibility features of AuNP1-dye-RBCM over AuNP1-dye. (f, g) Plots of SERS signal intensities at 1205 cm^{-1} as a function of storage time, showing the long-term stability of AuNP1-dye-RBCM over 2 weeks at 4 °C when compared to the original SERS nanotags (AuNP1-dye). Raman spectra were acquired at a laser power of 200 mW and integration time of 500 ms.

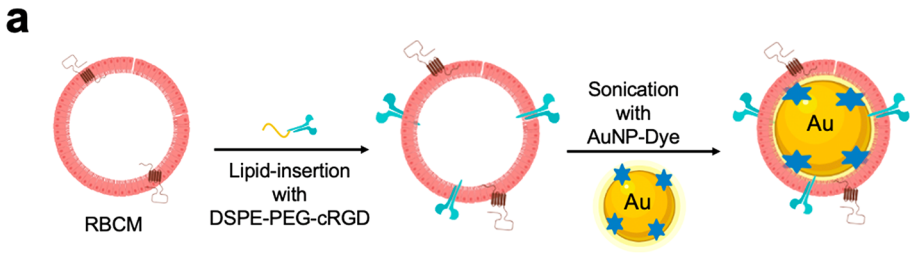

b

Samples	Hydrodynamic Diameter (nm)	Zeta Potential (mV)
AuNP-Dye	44 ± 7	-37 ± 6
RBCM	190 ± 22	-20 ± 8
RBCM@cRGD	194 ±15	-18 ± 4
AuNP-Dye-RBCM	64 ± 4	-28 ± 3
AuNP-Dye-RBCM@cRGD	68 ± 8	-25 ± 9

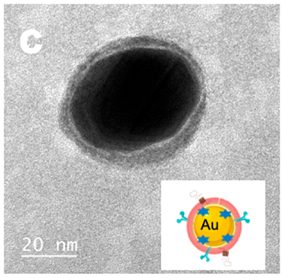

Figure 7. (a) Schematic showing the preparation of AuNP-dye-RBCMs with tumor targeting ability by lipid insertion. (b) Hydrodynamic diameter and ζ potential measurements of different samples. (c) Negative-stained TEM of AuNP1-dye-RBCM@cRGD.

We further demonstrated that the SERS signal for AuNP-dye-RBCM remains significantly stable (Figure S20) in the presence of serum proteins (50%), highlighting the importance of using these biomimetic SERS tags for different in vivo biosensing and biomedical applications.

Spectroscopic Detection of Cancer Cells Using Ligand-Inserted, Biomimetic SERS Nanoparticles. We next attempted to impart these biomimetic NPs with the cancer-targeting ability so that they could be used for in vitro SERS detection. A lipid-insertion strategy was adopted to functionalize RBCM with tumor-targeting peptides and subsequently coated them onto AuNPs. Toward this direction, we first attempted to optimize the lipid-insertion strategy in RBCM by using a lipid-tethered fluorescent probe (DSPE-PEG-Cy5, excitation/emission = 633 nm/660 nm). Fluorescent intensities were measured for DSPE-PEG-Cy5 at increasing concentrations (1–1000 μg/mL) to generate a calibration curve that would help us characterize the lipid-insertion efficiency and saturation level (Figure S21). Subsequently, DSPE-PEG-Cy5 at different concentrations was incubated with RBCM for 30 min at 4 °C followed by centrifugation, washing, referred to as RBCM-Cy5 1, 10, or 100 (depending on DSPE-PEG-Cy5 concentrations) and examined via fluorescence intensity measurements. Figure S22 demonstrates the ligand density on the RBCM by controlling the amount of lipid-tethered ligand added. We further demonstrated by flow cytometry that compared to unmodified RBCM, modified RBCM-Cy5 100 had a significantly higher signal under the Cy5 channel (Figure S23).

https://doi.org/10.1021/acsnano.2c01062
ACS Nano 2022, 16, 8051–8063

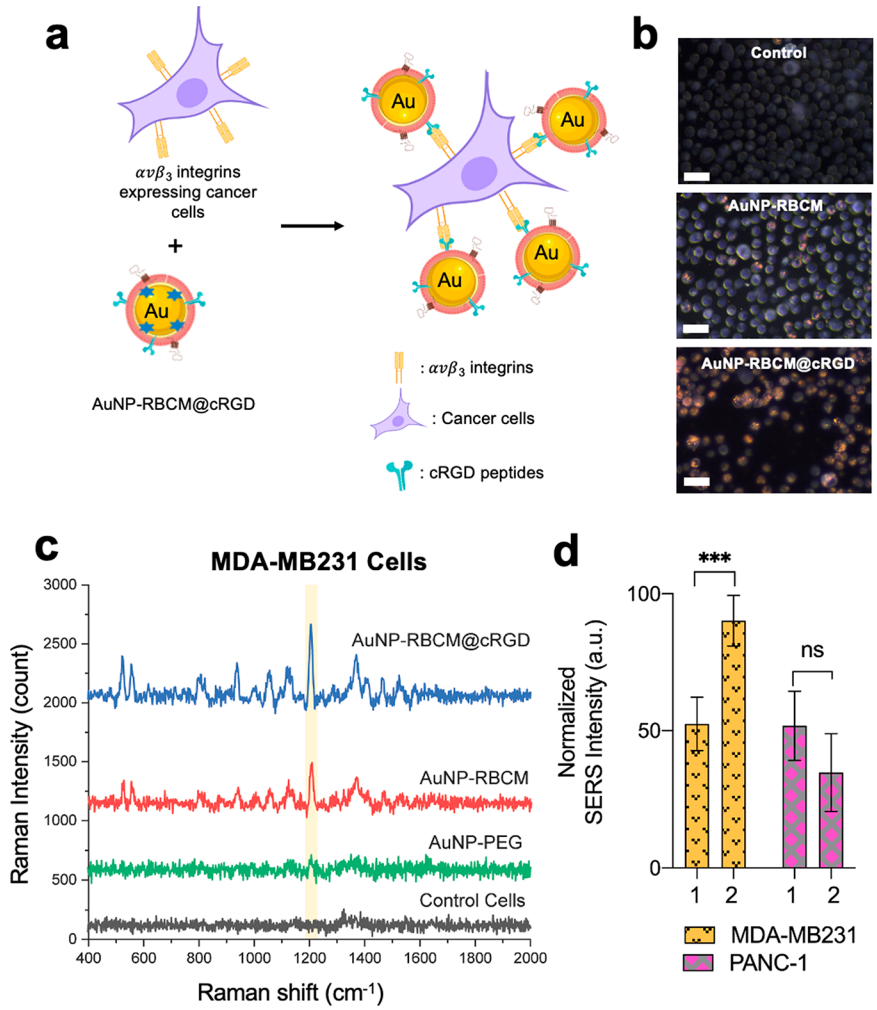

Figure 8. (a) Schematic depicting the targeting and spectroscopic detection of $\alpha v\beta 3$ expressing cancer cells using biomimetic and tumor targeted AuNP-RBCM@cRGD. (b) Dark-field microscopy images of MDA-MB231 cells incubated with PBS 1×, AuNP-RBCM, and AuNP-RBCM@cRGD, respectively. (c). Raman spectra of control cells, AuNP-PEG, AuNP-RBCM, and AuNP-RBCM@cRGD treated MDA-MB231 cells after overnight incubation. Each sample contains NP cell suspensions dispersed in PBS. Spectra were acquired at a laser power of 200 mW and the integration time of 2 s. (d) Normalized Raman intensity of (1) AuNP-RBCM and (2) AuNP-RBCM@cRGD treated cells at 1205 cm^{-1} Raman peak. MDA-MB231 and PANC-1 were selected as representative cell lines with and without cRGD targeted receptors, respectively.

Once we had validated the successful incorporation of lipid-tethered fluorescent dyes, we utilized a lipid-tethered tumor-targeting ligand (DSPE-PEG-cRGD) to functionalize AuNP-RBCM. Cancer targeting using NPs has been achieved in the last two decades by exploiting specific proteins that are upregulated in cancer cells. For example, integrins receptors are highly upregulated on tumor-associated endothelial cells during angiogenesis and metastasis of a wide range of rapidly growing tumors. Several integrins, including the αv integrins, have been shown to recognize the Arg-Gly-Asp (RGD) sequence as a critical determinant in their ligands. These RGD-functionalized nanocarriers have been extensively developed and utilized for tumor imaging and delivering cargoes (chemotherapeutics drugs). In this work, we attempted to selectively target $\alpha v\beta 3$ integrin-expressing cancer cells and their spectroscopic detection using lipid-inserted biomimetic SERS NPs (AuNP-RBCM). For cancer cell detection, cRGD-functionalized AuNP-RBCM were prepared using RBCM inserted with cRGD-PEG-lipid, followed by sonicating with AuNPs (Figure 7a,c). Hydrodynamic diameter and ζ potential values did not change appreciably before and after the lipid-insertion strategy (Figure 7b). UV−vis absorption spectroscopy was also conducted to show successful conjugation of cRGD peptides onto AuNP-RBCM. As the targeting ability of cRGD-functionalized NPs has been established in literature, we picked two model cancer cells lines, a high $\alpha v\beta 3$ integrin expressing cell line, MDA-MB231, and another with a low $\alpha v\beta 3$ integrin expressing cell line, PANC-1, to confirm successful functionalization. Prior to conducting in vitro SERS spectroscopy studies, the cellular viabilities of AuNP and AuNP-RBCM@cRGD were evaluated in MDA-MB231 and PANC-1 cell lines using the MTT assay and exhibited minimal cytotoxicity (Figure S24). After overnight incubation of the cells with different dye-tagged AuNPs (AuNP-PEG, AuNP-RBCM, and AuNP-RBCM@cRGD), cellular binding was evaluated using SERS spectroscopy and dark-field microscopy. The MDA-MB231 cells were $\alpha v\beta 3$ integrins positive and were detected with strong SERS signals (Figure 8a,c). In contrast, the PANC-1 cells did not express $\alpha v\beta 3$ integrins, showing little or minimal SERS signals (Figure 8d

https://doi.org/10.1021/acsnano.2c01062
ACS Nano 2022, 16, 8051−8063

and Figure S25). In addition, we further validated the in vitro targeting efficacy of AuNP-RBCM@cRGD in the endothelial cells using dark-field microscopy (Figure 8b). Dark-field imaging allows the generation of images from light scattering of the samples. AuNPs are detected for their increased scattering properties compared to the surrounding signals. For MDA-MB231 cells, AuNP-RBCM@cRGD appeared to bind with the cells at a high degree, unlike AuNP-RBCM which had minimal or low binding. Contrastingly, for PANC-1 cells, there was no enhanced binding among any of the investigated samples. Our results from SERS spectroscopy agree well with the expression levels of $\alpha v\beta 3$ integrins evaluated with the flow cytometry for these cells lines using FITC-conjugated mouse antibody, which show a high expression for MDA-MB231 cell line and low expression for PANC-1 cell line.[40,41]

CONCLUSION

In this report, we have shown that RBCM coatings impart a drastic enhancement in the dispersion stability of AuNPs, allowing AuNPs to be frozen, lyophilized, heated, or exposed to physiological conditions with superior performances than previous PEGylated SERS nanotags. Moreover, when the RBCM coating was applied to AuNPs functionalized with Raman-active dye molecules, it resulted in a further improvement in the particle brightness with excellent reproducibility, long-term retention of the signal intensity, and improved dispersion stability. These biomimetic SERS AuNPs were further modified with tumor-targeting peptides (cyclic-RGD) using a lipid-insertion strategy to target the $\alpha v\beta 3$ integrin receptors expressed on cancer cells and consequently used for in vitro SERS detection. Our data indicate that a biomimetic RBCM coating could be used as an alternative to PEGylated coating, imparting AuNPs with improved dispersibility, enhanced SERS signal brightness, and tumor targeting functions. We anticipate that biomimetic membranes of different origins (cancer cells, immune cells, bacteria, etc.) could be employed to impart plasmonic NPs with features of increased dispersion stability, improved SERS signal intensity, biocompatibility, and biofunctionalization capabilities for biomedical applications, facilitating their introduction at a clinical level.

METHODS

Materials. Deionized water (DI water) was used throughout the work. The following chemicals were used as purchased without any further purification: IR-780 iodide (dye content ≥95%), *N*,*N*-dimethylformamide (DMF), sodium citrate tribasic dihydrate, gold(III) chloride trihydrate ($HAuCl_4$), sodium borohydride ($NaBH_4$), poly(sodium 4-styrenesulfonate) (Na-PSS) solution (average Mw ~ 70,000, 30 wt %), silver nitrate ($AgNO_3$), L-ascorbic acid, sodium bromide (NaBr), hexadecyltrimethylammonium bromide (CTAB), and poly(ethylene glycol) methyl ether thiol (mPEG-thiol, Mn 2000 Da) from Sigma-Aldrich, hexadecyltrimethylammonium chloride (CTAC) from Tokyo Chemical Industry Co., Ltd., and poly(ethylene glycol) methyl ether thiol (mPEG-thiol, Mn 5000 Da) from Laysan Bio Inc.

Synthesis of Citrated-Stabilized Size and Shape Varied AuNPs. Glassware and stir bars for gold NP synthesis were washed by aqua regia before use. Gold nanospheres were synthesized via a kinetically controlled seeded growth method.[42] First, a water solution of 2.2 mM sodium citrate (60 mL) was heated to boiling under vigorous stirring. Once boiling had commenced, 400 μL of $HAuCl_4$ solution (25 mM) was quickly injected. The reaction completed within 10 min where the solution turned from yellow to purple gray and then to burgundy. Thirty mL of the resulting gold particle solution was stocked as 15 nm Au nanospheres (AuNP15), and the other 30 mL of the particle solution was used as the Au seeds for the next step. Immediately after the Au seeds synthesis, in the same reaction vessel, the solution was cooled to 90 °C, then 200 μL of $HAuCl_4$ solution (25 mM) was injected. After 30 min, the reaction was finished. This process was repeated once. After that, the particle solution was diluted two times by 2.2 mM sodium citrate solution. Thirty mL of the diluted particle solution was then used as the seed solution, and the process was repeated until Au nanospheres with a hydrodynamic size of 50 ± 5, 80 ± 5 nm in diameter were obtained sequentially, and the corresponding Au nanospheres solutions were stocked as AuNP45 and AuNP80, respectively. A condenser was utilized throughout the synthesis process to keep a consistent volume of the solution. The weight concentration of the obtained citrate stabilized Au nanospheres was determined by inductively coupled plasma mass spectrometry (ICP-MS). The size varied Au nanospheres solutions were finally diluted to 32 mg/L in 5 mM sodium citrate for long-term storage.

Gold nanorods (AuNP2) and gold nanocubes (AuNP3) were synthesized by seed-mediated growth methods.[43,44] A seed solution was first synthesized by quickly adding 600 μL of ice-cold 10 mM $NaBH_4$ solution to a mixed solution of CTAB (5 mL, 0.2 M) and $HAuCl_4$ (5 mL, 0.5 mM) under vigorous stirring. The seed solution was stirred for 2 min and then kept at room temperature for over 1 h before the next step. For the growth of nanorods, a CTAB solution (20 mL, 0.2 M) was first mixed with a $HAuCl_4$ solution (20 mL, 1 mM) and an $AgNO_3$ solution (1.2 mL, 4 mM) at a 30 °C water bath. To the above solution, 380 μL of 0.0788 M ascorbic acid solution was added, followed by gentle shaking. The growth solution was observed to change from yellow to colorless. After that, 48 μL of seed solution from the first step was added followed by gentle shaking, and the growth solution was kept at 30 °C unstirred. After 1 h, the growth was stopped by centrifuging the resulting AuNP2 solution at 4000*g*. The washed AuNP2 solution was redispersed to 2 mM CTAB solution.

For the synthesis of AuNP3, 10 nm gold nanospheres were first synthesized with the previously prepared CTAB-capped Au seeds. Two mL of 0.2 M CTAC solution, 1.5 mL of 0.1 M ascorbic acid solution, and 50 μL of the Au seeds solution were mixed in a 10 mL vial. Under stirring of constant speed, 2 mL of 0.5 mM $HAuCl_4$ solution was injected. The solution was incubated at room temperature for 15 min under stirring at 300 rpm. The resulting 10 nm Au nanosphere solution was then washed twice at 20,000*g* and redispersed to 1 mL in 20 mM CTAC solution for further use. For the growth of AuNP3, 72 mL of 0.1 M CTAC, 360 μL of 20 mM NaBr, and 84 μL of previously prepared 10 nm Au nanospheres were mixed, then 4.68 mL of a 10 mM ascorbic acid solution was added and mixed thoroughly. Finally, 72 mL of 0.5 mM $HAuCl_4$ solution was quickly injected into the solution under stirring at 500 rpm. The solution was incubated at room temperature for 30 min. The resulted AuNP3 solution was washed by centrifugation at 4000*g* and redispersed to 2 mM CTAC solution.

The surfactant exchange process of AuNP2 and AuNP3 follows a literature protocol.[45] Typically, 10 mL of AuNP2 or AuNP3 dispersed in 2 mM CTAB or CTAC solution was first centrifuged at 4000*g*. 9.5 mL of the supernatant was removed, and AuNP2 or AuNP3 were redispersed to 10 mL by DI water. The resulting AuNP2 or AuNP3 solution (current CTAB or CTAC concentration is 0.1 mM) was then added to 100 mL of Na-PSS solution (0.15 wt %) and kept at room temperature for over 1 h. After the incubation, the NP solution was centrifuged at 4000*g* and redispersed to 0.15 wt % Na-PSS solution for two cycles and then centrifuged again at 4000*g* and redispersed to 5 mM sodium citrate solution. The AuNPs were incubated in sodium citrate solution overnight. Finally, the AuNP2 or AuNP3 was washed again at 4000*g* by 5 mM sodium citrate. The concentrations of the citrate-stabilized AuNP2 and AuNP3 were determined by ICP-MS. The AuNP2 and AuNP3 solutions were finally diluted to 32 mg/L in 5 mM sodium citrate for long-term storage.

Synthesis of Shape Varied AuNP-PEGs. Typically, 3 mL of AuNPs solution (32 mg/L) was mixed with 500 μL of mPEG-thiol solution (51.8 μM) for 1 h at room temperature. The AuNPs were

https://doi.org/10.1021/acsnano.2c01062
ACS Nano 2022, 16, 8051−8063

then washed by DI water twice via centrifugation at 4000*g* to remove excess PEG ligands and redispersed to 3 mL of DI water.

RBCM Collection and Coating on AuNPs. RBCs derived from BALB/C mouse blood were purchased directly from BioIVT. Subsequently, it was subjected to hemolysis where the RBCs were suspended in lysis buffer, that is, 0.25× PBS at 4 °C for 1 h. The resulting solution was centrifuged 4 times at 20,000*g* to eliminate hemoglobin until a pink pellet (RBCM concentrate) was obtained and the supernatant solution was colorless. The pink pellet was resuspended in distilled water (∼50 mL) and vigorously mixed and sonicated for 10 min in ice−water mixture. The RBCM solution was eventually added to AuNP solution with the RBCM vesicle/AuNP volume ratio of 3/9 and bath sonicated for 10 min to form AuNP-RBCMs. The resulting solution was centrifuged at 700*g* for 15 min to eliminate residual RBCM vesicles aggregates.

Characterization of RBCM-Coated Nanoparticles. Dynamic light scattering (DLS) measurements were conducted to measure the hydrodynamic size distribution (intensity average) of the NPs on Malvern Zetasizer ZS90 instrument (Malvern Instruments Ltd., United Kingdom) at a fixed angle of 90°. The ζ potential values were determined using a Malvern Zetasizer (Malvern Instruments Ltd., United Kingdom) of Nano series. UV−vis absorbance was recorded on GENESYSTM 10S UV−vis spectrophotometer (Thermo Scientific, MA, USA). Absorbance spectra were collected at an interval of 1 nm scanning from 300 nm to 1000 nm. To evaluate the presence of CD47 on the surface of the particle, allophycocyanin-labeled antimouse CD47 antibody was used (BioLegend, San Diego, CA) according to a previously established protocol.[30]

Transmission Electron Microscopy Imaging. A drop of RBC-coated or bare (non-RBC-coated) NP solution was deposited onto a glow-discharged, carbon-coated transmission electron microscopy (TEM) grid and incubated for 5 min. Excess liquid was removed, and samples dried overnight in a desiccation chamber. For negative staining, samples were stained with 1% uranyl acetate for 30 s immediately before imaging. All samples were imaged using a JEOL JEM-2100 transmission electron microscope at 200 kV.

Dispersion Stability against Freeze−Thaw Cycle. AuNPs having different shapes and sizes with citrates only, RBCM coating, and PEG coating, respectively, were taken in glass vials (2 mL, 0.032 mg/mL). The resulting solutions were frozen at −80 °C for 30 min and then thawed at room temperature for 10 min. The thawed solutions were briefly sonicated and analyzed using UV−vis spectrophotometry and DLS.

Dispersion Stability against Lyophilization. AuNPs having different shapes and sizes with citrates only, RBCM coating, and PEG coating, respectively, were taken in glass vials (2 mL, 0.032 mg/mL). The resulting solutions were frozen by placing them in liquid nitrogen for a few minutes and then connected immediately to a freeze-drier (−47 °C) with an applied vacuum (53×10^{-4} mbar) for ∼24 h. The freeze-dried products were reconstituted with deionized water (1 mL). The NP solutions were briefly sonicated and analyzed using UV−vis spectrophotometry and DLS.

Dispersion Stability against Heating. AuNP1s with citrate only, RBCM coating, and PEG coating were placed in glass vials (2 mL, 0.032 mg/mL). The resulting solutions were placed with caps to prevent evaporation of water and subsequently were heated for 4 h at 85 °C. Following that, they were briefly sonicated and analyzed by collecting time-course UV−vis measurement.

Dispersion Stability against a PBS Buffer Solution. AuNP1s with citrate only, RBCM coating, and PEG coating were placed in glass vials (2 mL, 0.032 mg/mL). A 0.1 mL phosphate-buffered saline (PBS) solution (pH = 7.4, KCl = 2.6 mM, KH_2PO_4 = 1.47 mM, NaCl = 137.9 mM) was added to each vial. Time-course UV−vis measurements were taken before and after the addition of the PBS solution.

Stability of AuNPs in Human Serum. AuNPs were added to undiluted human serum in a ratio of 1:1 (final solution containing 50% serum). The samples were incubated for 24 h at 37 °C. Samples were then centrifuged at 10,000 rpm, and the dispersion solution was removed. The AuNPs were resuspended in distilled water and centrifuged down at 10,000 rpm; this process was repeated twice. Finally, DLS profiles of AuNPs in water were recorded using a Malvern Zetasizer Nano ZS.

AuNP-Dye Physisorption for SERS Studies. Raman reporter dyes were physically attached to AuNPs before the PEG or RBCM coating process. Raman reporter molecules IR-780 stock solution were prepared by dissolving 1 mg of IR-780 into 1 mL of DMF. The stock solutions were diluted by DI water to form a dye concentration of 2.62 μM for further use. Typically, 10 μL above IR-780 solution was dropwise added to 1 mL of gold AuNP1 (32 mg/L) under vigorous stirring. The resulting dye concentration for 45 nm gold AuNP1 was calculated to be 450 dye molecules per AuNP.

SERS Data Collection and Processing. Raman spectra were obtained using a BaySpec Agility transportable 785/1064 nm dual-band benchtop Raman spectrometer (East JHX, Inc.). A 785 nm laser (200 mW) was used as the excitation source. Each Raman measurement includes 3 scans, and the averaged Raman spectrum was plotted. Averaged Raman intensity of 1205 cm^{-1} peak from the 3 scans was chosen to show the Raman signal change for the SERS AuNPs, and the error bars represent the standard deviations of the scans performed for 3 separate experiments. All the Raman spectra were baseline corrected to remove fluorescence background, and the band intensities were calibrated by standard sample (benzonitrile) spectrum.

Lipid Insertion of Tumor-Targeting Peptides. Stock solutions of DSPE-PEG-Cy5 with concentrations (1000 μg/mL, 500 μg/mL, 200 μg/mL, 100 μg/mL, 50 μg/mL, 10 μg/mL, and 1 μg/mL) were made in DI water. RBCMs prepared earlier were thawed and bath-sonicated in ice water. Subsequently, 1 mL of RBCM was added to 1 mL of each DSPE-PEG-Cy5 of different concentrations and vortexed vigorously for 1 min. The solutions were incubated for 30 min in the refrigerator followed by centrifugation at 600*g* for 15 min at 4 °C. The supernatant was removed, and 2 mL of DI water was added to each tube. The UV−vis absorption was collected in addition to acquiring their fluorescence excitation and emission spectra at 633 nm and 650−700 nm, respectively.

MTT Assay of Different AuNPs. The cytotoxic effects of various AuNPs in two different endothelial cell lines (MDA-MB231, PANC-1) were investigated using MTT assay established previously.[46−48]

In Vitro SERS Study. To verify the effective binding of AuNP-RBCM@cRGD to endothelial cells, a comparative targeting study was performed in vitro with MDA-MB231 and PANC-1 cells. Both cell lines were grown in Eagle's minimum essential medium (MEM), supplemented with 1.5 g/L sodium bicarbonate, nonessential amino acids, L-glutamine, and sodium pyruvate and cultured until they reached ∼80−90% confluency. Subsequently, they were plated in a 6-well plate at a density of 10^6 cells per well and allowed to grow for 24 h at 37 °C. Dye-tagged AuNPs (AuNP-PEG, AuNP-RBCM, and AuNP-RBCM@cRGD) were added to the media and allowed to incubate overnight. Following this, the AuNP-containing media was removed by aspiration, and cells were rinsed two times with PBS. The cells were then collected and measured for SERS signal intensities using a BaySpec Agility transportable 785/1064 nm dual-band benchtop Raman spectrometer (East JHX, Inc.). Subsequently, the same cell samples were fixed with Karnovsky's fixative (paraformaldehyde-glutaraldehyde solution) and imaged using dark-field microscopy to visualize the AuNPs associated with the cells. Dark-field microscopy was performed using a Zeiss Axiovert inverted microscope. All images were acquired using a 50× objective lens.

ASSOCIATED CONTENT

Supporting Information

The Supporting Information is available free of charge at https://pubs.acs.org/doi/10.1021/acsnano.2c01062.

Further details on enhancement factor calculations, and 25 figures of experimental data showing: (1) UV−vis absorption spectra of PEGylated AuNPs, (2) improved dispersion stability of various size and anisotropic

https://doi.org/10.1021/acsnano.2c01062
ACS Nano 2022, 16, 8051−8063

AuNPs, (3) negative-stained TEM, (4) physiological stability data of AuNP-RBCMs, (5) SERS signal stability data of AuNPs upon freeze−thaw and lyophilization cycles, (6) lipid-insertion optimization data, (7) cellular toxicity data of AuNP-RBCMs, and (8) in vitro SERS spectra of AuNP-RBCMs in PANC-1 cells (PDF)

AUTHOR INFORMATION

Corresponding Authors

Shuming Nie − *Department of Bioengineering, Department of Electrical and Computer Engineering, Department of Materials Science and Engineering, Department of Chemistry, and Carle Illinois College of Medicine, University of Illinois at Urbana−Champaign, Urbana, Illinois 61801, United States;* orcid.org/0000-0002-7328-1144; Email: nies@illinois.edu

Viktor Gruev − *Department of Electrical and Computer Engineering and Carle Illinois College of Medicine, University of Illinois at Urbana−Champaign, Urbana, Illinois 61801, United States*; Email: vgruev@illinois.edu

Authors

Indrajit Srivastava − *Department of Bioengineering and Department of Electrical and Computer Engineering, University of Illinois at Urbana−Champaign, Urbana, Illinois 61801, United States;* orcid.org/0000-0002-6864-0202

Ruiyang Xue − *Department of Materials Science and Engineering, University of Illinois at Urbana−Champaign, Urbana, Illinois 61801, United States*

Jamie Jones − *Department of Bioengineering, University of Illinois at Urbana−Champaign, Urbana, Illinois 61801, United States*

Hyunjoon Rhee − *Department of Bioengineering, University of Illinois at Urbana−Champaign, Urbana, Illinois 61801, United States*

Kristen Flatt − *Materials Research Laboratories Central Research Facilities, University of Illinois at Urbana−Champaign, Urbana, Illinois 61801, United States*

Complete contact information is available at: https://pubs.acs.org/10.1021/acsnano.2c01062

Author Contributions

I.S. conceived the concept and designed all the experiments. R.X. performed AuNP synthesis and characterized them. I.S. performed and optimized the RBCM coating, lipid insertion studies, conducted in vitro studies, and analyzed the data. J.J. was trained by I.S. and performed RBCM coating, lipid insertion studies, and in vitro studies. I.S., H.R., and J.J. performed the enhanced dispersibility studies and analyzed the data. R.X. and I.S. performed SERS measurements and analyzed the data. K.F. performed the negative-stained transmission electronic microscopy images. S.N. provided important theoretical and experimental insights and supervised the overall project. I.S. and S.N. wrote the manuscript with further editing by R.X., J. J., K.F., and V.G. All authors have given approval to the final version of the manuscript.

Notes

The authors declare no competing financial interest.

ACKNOWLEDGMENTS

S.N. acknowledges the Grainger College of Engineering and the University of Illinois at Urbana−Champaign for institutional support. V.G. thanks the Congressionally Directed Medical Research Program (grant W81XWH-19-1-0299) and the National Science Foundation (grant 2030421). I.S. acknowledges the Baxter Young Investigator Award. The authors thank Dr. Julio Soares for assistance with dark-field microscopy imaging. Transmission electron microscopy and dark-field microscopy imaging was carried out in the Materials Research Laboratory Central Research Facilities, University of Illinois.

REFERENCES

(1) Mulvaney, S. P.; Musick, M. D.; Keating, C. D.; Natan, M. J. Glass-coated, analyte-tagged nanoparticles: a new tagging system based on detection with surface-enhanced Raman scattering. *Langmuir* **2003**, *19* (11), 4784−4790.

(2) Fernández-López, C.; Mateo-Mateo, C.; Álvarez-Puebla, R. A.; Pérez-Juste, J.; Pastoriza-Santos, I.; Liz-Marzán, L. M. Highly controlled silica coating of PEG-capped metal nanoparticles and preparation of SERS-encoded particles. *Langmuir* **2009**, *25* (24), 13894−13899.

(3) Rodríguez-Lorenzo, L.; Krpetic, Z.; Barbosa, S.; Alvarez-Puebla, R. A.; Liz-Marzán, L. M.; Prior, I. A.; Brust, M. Intracellular mapping with SERS-encoded gold nanostars. *Integrative Biology* **2011**, *3* (9), 922−926.

(4) Rodríguez-Fernández, D.; Langer, J.; Henriksen-Lacey, M.; Liz-Marzán, L. M. Hybrid Au-SiO2 core-satellite colloids as switchable SERS tags. *Chem. Mater.* **2015**, *27* (7), 2540−2545.

(5) Mir-Simon, B.; Reche-Perez, I.; Guerrini, L.; Pazos-Perez, N.; Alvarez-Puebla, R. A. Universal one-pot and scalable synthesis of SERS encoded nanoparticles. *Chem. Mater.* **2015**, *27* (3), 950−958.

(6) Stokes, R. J.; Hernandez-Santana, A.; Macaskill, A.; Cormack, P. A. G.; Smith, W. E.; Graham, D. SERRS-active nanoparticle-polymer beads for ultra-sensitive biodiagnostic applications. *Micro and Nano Letters* **2006**, *1* (1), 57−61.

(7) McLintock, A.; Hunt, N.; Wark, A. W. Controlled side-by-side assembly of gold nanorods and dye molecules into polymer-wrapped SERRS-active clusters. *Chem. Commun.* **2011**, *47* (13), 3757−3759.

(8) Bodelõn, G.; Montes-García, V.; Fernández-Lõpez, C.; Pastoriza-Santos, I.; Pérez-Juste, J.; Liz-Marzán, L. M. Au@pNIPAM SERRS Tags for Multiplex Immunophenotyping Cellular Receptors and Imaging Tumor Cells. *Small* **2015**, *11* (33), 4149−4157.

(9) Soliman, M. G.; Pelaz, B.; Parak, W. J.; Del Pino, P. Phase transfer and polymer coating methods toward improving the stability of metallic nanoparticles for biological applications. *Chem. Mater.* **2015**, *27* (3), 990−997.

(10) Song, J.; Zhou, J.; Duan, H. Self-assembled plasmonic vesicles of SERS-encoded amphiphilic gold nanoparticles for cancer cell targeting and traceable intracellular drug delivery. *J. Am. Chem. Soc.* **2012**, *134* (32), 13458−13469.

(11) Ip, S.; MacLaughlin, C. M.; Gunari, N.; Walker, G. C. Phospholipid membrane encapsulation of nanoparticles for surface-enhanced raman scattering. *Langmuir* **2011**, *27* (11), 7024−7033.

(12) Tam, N. C. M.; Scott, B. M. T.; Voicu, D.; Wilson, B. C.; Zheng, G. Facile synthesis of raman active phospholipid gold nanoparticles. *Bioconjugate Chem.* **2010**, *21* (12), 2178−2182.

(13) Tam, N. C. M.; McVeigh, P. Z.; MacDonald, T. D.; Farhadi, A.; Wilson, B. C.; Zheng, G. Porphyrin-lipid stabilized gold nanoparticles for surface enhanced Raman scattering based imaging. *Bioconjugate Chem.* **2012**, *23* (9), 1726−1730.

(14) Wang, L. Y.; Wang, S. G.; Bei, J. Z. Synthesis and characterization of macroinitiator-amino terminated PEG and poly-(γ-benzyl-L-glutamate)-PEO-poly(γ-benzyl-L-glutamate triblock co-polymer. *Polym. Adv. Technol.* **2004**, *15* (10), 617−621.

(15) Akagi, T.; Higashi, M.; Kaneko, T.; Kida, T.; Akashi, M. Hydrolytic and enzymatic degradation of nanoparticles based on amphiphilic poly(γ-glutamic acid)-graft-L-phenylalanine copolymers. *Biomacromolecules* **2006**, *7* (1), 297−303.
(16) Sekiguchi, S.; Niikura, K.; Matsuo, Y.; Ijiro, K. Hydrophilic gold nanoparticles adaptable for hydrophobic solvents. *Langmuir* **2012**, *28* (13), 5503−5507.
(17) Zhang, G.; Yang, Z.; Lu, W.; Zhang, R.; Huang, Q.; Tian, M.; Li, L.; Liang, D.; Li, C. Influence of anchoring ligands and particle size on the colloidal stability and in vivo biodistribution of polyethylene glycol-coated gold nanoparticles in tumor-xenografted mice. *Biomaterials* **2009**, *30* (10), 1928−1936.
(18) Alkilany, A. M.; Abulateefeh, S. R.; Mills, K. K.; Bani Yaseen, A. I.; Hamaly, M. A.; Alkhatib, H. S.; Aiedeh, K. M.; Stone, J. W. Colloidal stability of citrate and mercaptoacetic acid capped gold nanoparticles upon lyophilization: Effect of capping ligand attachment and type of cryoprotectants. *Langmuir* **2014**, *30* (46), 13799−13808.
(19) Gupta, A.; Moyano, D. F.; Parnsubsakul, A.; Papadopoulos, A.; Wang, L. S.; Landis, R. F.; Das, R.; Rotello, V. M. Ultrastable and Biofunctionalizable Gold Nanoparticles. *ACS Appl. Mater. Interfaces* **2016**, *8* (22), 14096−14101.
(20) Ip, S.; MacLaughlin, C. M.; Joseph, M.; Mullaithilaga, N.; Yang, G.; Wang, C.; Walker, G. C. Dual-Mode Dark Field and Surface-Enhanced Raman Scattering Liposomes for Lymphoma and Leukemia Cell Imaging. *Langmuir* **2019**, *35* (5), 1534−1543.
(21) Hu, C.-M. J.; Zhang, L.; Aryal, S.; Cheung, C.; Fang, R. H.; Zhang, L. Erythrocyte membrane-camouflaged polymeric nanoparticles as a biomimetic delivery platform. *Proc. Natl. Acad. Sci. U. S. A.* **2011**, *108* (27), 10980−10985.
(22) Holay, M.; Zhou, J.; Park, J. H.; Landa, I.; Ventura, C. J.; Gao, W.; Fang, R. H.; Zhang, L. Organotropic Targeting of Biomimetic Nanoparticles to Treat Lung Disease. *Bioconjugate Chem.* **2022**, *33*, 586.
(23) Hu, C. M. J.; Fang, R. H.; Copp, J.; Luk, B. T.; Zhang, L. A biomimetic nanosponge that absorbs pore-forming toxins. *Nat. Nanotechnol.* **2013**, *8* (5), 336−340.
(24) Wang, F.; Gao, W.; Thamphiwatana, S.; Luk, B. T.; Angsantikul, P.; Zhang, Q.; Hu, C. M. J.; Fang, R. H.; Copp, J. A.; Pornpattananangkul, D.; Lu, W.; Zhang, L. Hydrogel retaining toxin-absorbing nanosponges for local treatment of methicillin-resistant Staphylococcus aureus infection. *Adv. Mater.* **2015**, *27* (22), 3437−3443.
(25) Zinger, A.; Sushnitha, M.; Naoi, T.; Baudo, G.; De Rosa, E.; Chang, J.; Tasciotti, E.; Taraballi, F. Enhancing Inflammation Targeting Using Tunable Leukocyte-Based Biomimetic Nanoparticles. *ACS Nano* **2021**, *15* (4), 6326−6339.
(26) Li, J.; Angsantikul, P.; Liu, W.; Esteban-Fernández de Ávila, B.; Chang, X.; Sandraz, E.; Liang, Y.; Zhu, S.; Zhang, Y.; Chen, C.; Gao, W.; Zhang, L.; Wang, J. Biomimetic Platelet-Camouflaged Nanorobots for Binding and Isolation of Biological Threats. *Adv. Mater.* **2018**, *30* (2), 1704800.
(27) Fang, R. H.; Hu, C. M. J.; Chen, K. N. H.; Luk, B. T.; Carpenter, C. W.; Gao, W.; Li, S.; Zhang, D. E.; Lu, W.; Zhang, L. Lipid-insertion enables targeting functionalization of erythrocyte membrane-cloaked nanoparticles. *Nanoscale* **2013**, *5* (19), 8884−8888.
(28) Hu, C. M. J.; Zhang, L.; Aryal, S.; Cheung, C.; Fang, R. H.; Zhang, L. Erythrocyte membrane-camouflaged polymeric nanoparticles as a biomimetic delivery platform. *Proc. Natl. Acad. Sci. U.S.A.* **2011**, *108* (27), 10980−10985.
(29) Gao, W.; Hu, C. M. J.; Fang, R. H.; Luk, B. T.; Su, J.; Zhang, L. Surface functionalization of gold nanoparticles with red blood cell membranes. *Adv. Mater.* **2013**, *25* (26), 3549−3553.
(30) Ben-Akiva, E.; Meyer, R. A.; Yu, H.; Smith, J. T.; Pardoll, D. M.; Green, J. J. Biomimetic anisotropic polymeric nanoparticles coated with red blood cell membranes for enhanced circulation and toxin removal. *Science Advances* **2020**, *6* (16), No. eaay9035.
(31) Nam, S.; Parikh, D. V.; Condon, B. D.; Zhao, Q.; Yoshioka-Tarver, M. Importance of poly(ethylene glycol) conformation for the synthesis of silver nanoparticles in aqueous solution. *J. Nanopart. Res.* **2011**, *13* (9), 3755−3764.
(32) Boisselier, E.; Astruc, D. Gold nanoparticles in nanomedicine: preparations, imaging, diagnostics, therapies and toxicity. *Chem. Soc. Rev.* **2009**, *38* (6), 1759−1782.
(33) Jiang, Y.; Huo, S.; Mizuhara, T.; Das, R.; Lee, Y. W.; Hou, S.; Moyano, D. F.; Duncan, B.; Liang, X. J.; Rotello, V. M. The Interplay of Size and Surface Functionality on the Cellular Uptake of Sub-10 nm Gold Nanoparticles. *ACS Nano* **2015**, *9* (10), 9986−9993.
(34) Wang, Y.; Quinsaat, J. E. Q.; Ono, T.; Maeki, M.; Tokeshi, M.; Isono, T.; Tajima, K.; Satoh, T.; Sato, S. I.; Miura, Y.; Yamamoto, T. Enhanced dispersion stability of gold nanoparticles by the physisorption of cyclic poly(ethylene glycol). *Nat. Commun.* **2020**, *11* (1), 6089.
(35) Manson, J.; Kumar, D.; Meenan, B. J.; Dixon, D. Polyethylene glycol functionalized gold nanoparticles: the influence of capping density on stability in various media. *Gold Bulletin* **2011**, *44* (2), 99−105.
(36) Schatz, G. C.; Young, M. A.; Van Duyne, R. P. Electromagnetic mechanism of SERS. In *Surface-Enhanced Raman Scattering, Topics in Applied Physics*; Kneipp, K., Moskovits, M., Kneipp, H., Eds.; Springer: Berlin, Heidelberg, 2006; Vol. *103*, pp 19−46.
(37) Kleinman, S. L.; Frontiera, R. R.; Henry, A. I.; Dieringer, J. A.; Van Duyne, R. P. Creating, characterizing, and controlling chemistry with SERS hot spots. *Phys. Chem. Chem. Phys.* **2013**, *15* (1), 21−36.
(38) Lee, H. K.; Lee, Y. H.; Koh, C. S. L.; Phan-Quang, G. C.; Han, X.; Lay, C. L.; Sim, H. Y. F.; Kao, Y. C.; An, Q.; Ling, X. Y. Designing surface-enhanced Raman scattering (SERS) platforms beyond hotspot engineering: Emerging opportunities in analyte manipulations and hybrid materials. *Chem. Soc. Rev.* **2019**, *48* (3), 731−756.
(39) Nam, J. M.; Oh, J. W.; Lee, H.; Suh, Y. D. Plasmonic Nanogap-Enhanced Raman Scattering with Nanoparticles. *Acc. Chem. Res.* **2016**, *49* (12), 2746−2755.
(40) Ji, S.; Xu, J.; Zhang, B.; Yao, W.; Xu, W.; Wu, W.; Xu, Y.; Wang, H.; Ni, Q.; Hou, H.; Yu, X. RGD-conjugated albumin nanoparticles as a novel delivery vehicle in pancreatic cancer therapy. *Cancer Biology and Therapy* **2012**, *13* (4), 206−215.
(41) Stojanovic, N.; Dekanic, A.; Paradžik, M.; Majhen, D.; Ferenčak, K.; Ruščic, J.; Bardak, I.; Supina, C.; Tomicic, M. T.; Christmann, M.; Osmak, M.; Ambriović-Ristov, A. Differential effects of integrin av knockdown and cilengitide on sensitization of triple-negative breast cancer and melanoma cells to microtubule poisons. *Mol. Pharmacol.* **2018**, *94* (6), 1334−1351.
(42) Bastús, N. G.; Comenge, J.; Puntes, V. Kinetically controlled seeded growth synthesis of citrate-stabilized gold nanoparticles of up to 200 nm: Size focusing versus ostwald ripening. *Langmuir* **2011**, *27* (17), 11098−11105.
(43) Park, J. E.; Lee, Y.; Nam, J. M. Precisely Shaped, Uniformly Formed Gold Nanocubes with Ultrahigh Reproducibility in Single-Particle Scattering and Surface-Enhanced Raman Scattering. *Nano Lett.* **2018**, *18* (10), 6475−6482.
(44) Nikoobakht, B.; El-Sayed, M. A. Preparation and growth mechanism of gold nanorods (NRs) using seed-mediated growth method. *Chem. Mater.* **2003**, *15* (10), 1957−1962.
(45) Mehtala, J. G.; Zemlyanov, D. Y.; Max, J. P.; Kadasala, N.; Zhao, S.; Wei, A. Citrate-stabilized gold nanorods. *Langmuir* **2014**, *30* (46), 13727−13730.
(46) Srivastava, I.; Misra, S. K.; Ostadhossein, F.; Daza, E.; Singh, J.; Pan, D. Surface chemistry of carbon nanoparticles functionally select their uptake in various stages of cancer cells. *Nano Research* **2017**, *10* (10), 3269−3284.
(47) Srivastava, I.; Misra, S. K.; Bangru, S.; Boateng, K. A.; Soares, J. A. N. T.; Schwartz-Duval, A. S.; Kalsotra, A.; Pan, D. Complementary Oligonucleotide Conjugated Multicolor Carbon Dots for Intracellular Recognition of Biological Events. *ACS Appl. Mater. Interfaces* **2020**, *12* (14), 16137−16149.
(48) Srivastava, I.; Moitra, P.; Fayyaz, M.; Pandit, S.; Kampert, T. L.; Fathi, P.; Alanagh, H. R.; Dighe, K.; Alafeef, M.; Vuong, K.; Jabeen, M.; Nie, S.; Irudayaraj, J.; Pan, D. Rational Design of Surface-State

https://doi.org/10.1021/acsnano.2c01062
ACS Nano 2022, 16, 8051−8063

Controlled Multicolor Cross-Linked Carbon Dots with Distinct Photoluminescence and Cellular Uptake Properties. *ACS Appl. Mater. Interaces* **2021**, *13* (50), 59747−59760.

https://doi.org/10.1021/acsnano.2c01062
ACS Nano 2022, 16, 8051−8063